2012 American Control Conference
Fairmont Queen Elizabeth, Montréal, Canada
June 27-June 29, 2012

Formation Flight of Unmanned Rotorcraft Based on Robust and Perfect Tracking Approach

Biao Wang[1], Xiangxu Dong[1], Ben M. Chen[1], Tong H. Lee[1], Swee King Phang[2]

Abstract— **The paper presents a control scheme to the formation flight of a pair of unmanned rotorcraft. A leader-follower formation strategy is adopted and it is realized by utilizing the robust and perfect tracking (RPT) control approach. More specifically, individual RPT flight control laws are implemented in each aircraft, while the measurements from its neighbor and its own sensors are both taken into account for feedback to each aircraft system. In addition, a formation command generator is executed on the follower to ensure that it remains in formation with the leader. This control scheme facilitates the construction of formation flight systems and eases the changing of formation scale. Finally, the proposed formation flight strategy is realized and its performance is verified through several flight tests.**

I. INTRODUCTION

The coordinated movements of animals such as flocks of birds and schools of fish without colliding with each other exhibit the robust biological systems with stable formation behavior [1]. Motivated by this natural behavior, concept of coordinated movements has been implemented in various artificial systems, such as unmanned aerial vehicles (UAVs). To date, it is widely believed that a group of well-organized low-cost UAVs can be far superior to a single high-technology and high-cost UAV in term of effectiveness [2]. For example, in-flight refueling between UAVs enables longer flight duration and distance. Flight formation can also increase the efficiency of missions such as surveillance and reconnaissance, delivery of payloads, and pesticide scattering. With the progress in the development of low-cost UAVs, there is an obvious growing interest in applications for UAVs formation flight [3]. In this paper, we focus on the formation flight of multiple unmanned rotorcraft.

Formation flight has been investigated before the 90s of the last century for manned aircraft including both airplanes (fixed-wing aircraft) and helicopters. A supporting system was developed for manned aircraft in formation flight in [4] to facilitate the operation of human pilots in rendezvous, joinup, collision avoidance, formation flight, and fail safe. Early 1990s, automatic formation flight became an important topic for airplanes due to drag reduction (see e.g., [5], [6], [7]). Since then, NASA has conducted autonomous formation flight (AFF) tests using a pair of F/A-18 aircraft [8]. West Virginia University demonstrated AFF using three YF-22 research airplanes [9]. Recently, AFF has been widely studied to be adapted in miniature low-cost unmanned rotorcraft [3], [10], [11], [12], [13], [14].

In general, there are three formation strategies: trajectory tracking, leader-follower, and behavioral approach (or virtual structure) [9], [15], [16], [17]. This paper focuses solely on the second strategy, which works based on the relative position errors between the aircraft in formation. It is most commonly used to track arbitrary maneuvering and is studied most widely due to its practical meaning. This strategy can be divided into two modes [16]: the front mode and the leader mode. The former allows a trailing aircraft (named wingman) follows only its nearest neighbor in front, whereas the latter restricts all the trailing aircraft in formation to follow their group leader without considering their neighbors.

Different control schemes and techniques have been applied to formation control problems [1], [15], [18], [19]. A centralized controller could theoretically deliver stability and performance but would impose high computation and communication costs. Furthermore, the controller would have to be tailored to each specific formation. For instant, if the number of followers in a formation were to change, the controller will need to be revised completely. A purely decentralized control, in which the formation-keeping autopilots of the various aircraft do not communicate, may fail to counteract the instability where control based on more information about the structure of the system would succeed. Distributed control scheme may seek a compromise solution. Based on these schemes, wide variety of control methods have been applied to solve the formation problem, such as classic PID control, sliding-model control, model predictive control, robust control, dynamic inversion, etc.

Most of the works for formation flight mentioned above are verified only by simulation. In this paper, we will present our solution with real data obtained from flight tests. The main contribution of our work is the physically applicable and straightforward way to construct flight formation system. The solution scheme includes position, velocity and even acceleration matching between aircraft to achieve a good formation performance. It eases the changing of formation scale. With the objective of producing a prototype system of formation flight, we start our study with station-keeping formation flight involving only one leader-follower pair. It is the element of larger formations. To realize our solution, two unmanned helicopters developed by the UAV research team from the National University of Singapore (http://uav.ece.nus.edu.sg) codenamed HeLion (leader) and SheLion (follower) as shown in Fig. 1 will be utilized.

The outline of the paper is as follows. Section II discusses

[1]B. Wang, X. Dong, B. M. Chen, and T. H. Lee are with the Department of Electrical and Computer Engineering, National University of Singapore, Singapore 117576 wangbiao@nuaa.edu.cn, {dong07, bmchen, eleleeth}@nus.edu.sg

[2]S. K. Phang is with the NUS Graduate School (NGS) for Integrative Sciences and Engineering, National University of Singapore, Singapore 117456 a0033585@nus.edu.sg

978-1-4577-1094-0/12/$26.00 ©2012 AACC

Fig. 1. NUS HeLion and SheLion in formation flight

the selection of coordinate systems for formation flight of helicopters. Section III presents the problem formulation of formation flight and layouts the solution scheme, whereas Section IV details the generation of formation command via deriving the formation dynamics. The actual flight test results and performance analysis of our design are given in Section V. Finally, Section VI draws some concluding remarks.

II. Frames of Reference and Coordinate Systems

Frames of reference and coordinate systems must be selected carefully for three dimensional formation flight. They will affect the motion pattern of formation flight and even the feasibility of control system design in practice. Considering that formation is the behavior of individuals relative to the team leader or neighbors, a body-carried moving frame of reference is necessary to define the configuration. The most widely used description to a body-carried frame is the body-axis coordinate system. As the definition of formation flight, the follower is to maintain at a constant distance relative to the leader's frame. Thus it is not feasible to utilize the body-axis coordinate system as pitch and roll motion of the leader will cause unwanted movement to the follower.

In this paper, we define a new coordinate system for the formation configuration of helicopters–the *heading coordinate system*. To setup the coordinate system, a north-east-down (NED) frame is fixed at the locations where each aircraft is powered up; its x-, y- and z-axes locally point to north, east and down, respectively. With this assignment, each aircraft has its own fixed-NED coordinate system, which has similar orientation and different in position. Then, on each aircraft's center of gravity o_b, we define a body-carried NED coordinate system ($o_\mathrm{b}x_\mathrm{n}y_\mathrm{n}z_\mathrm{n}$), a body-axis coordinate system ($o_\mathrm{b}x_\mathrm{b}y_\mathrm{b}z_\mathrm{b}$), and a heading coordinate system ($o_\mathrm{b}x_\mathrm{h}y_\mathrm{h}z_\mathrm{h}$). In this paper, it is reasonable to assume that all the NED coordinate systems have the same orientation. The body-axis coordinate system is defined same as the most of the literature in aeronautics. For the heading coordinate system, its x_h-axis coincides with the projection of x_b-axis on the local horizontal plane, z_h-axis points vertically downward, y_h-axis lies in the horizontal plane perpendicular to the x_h-z_h plane under the right-hand rule. In other words, it is a coordinate system rotating $x_\mathrm{n}y_\mathrm{n}z_\mathrm{n}$ by the heading angle ψ of the aircraft. The frames allocation can be visualized in Fig. 2.

In our implementation, the leader's heading coordinate system is chosen as the reference of formation configuration. Since it rotates only around the z_n-axis, the coordinate conversion from the leader's heading coordinate system to the leader's body-carried NED coordinate system can be expressed as

$$(x_\mathrm{n}, y_\mathrm{n}, z_\mathrm{n})^\mathrm{T} = \mathbf{R}_{\psi_\mathrm{L}}(x_\mathrm{h}, y_\mathrm{h}, z_\mathrm{h})^\mathrm{T} \tag{1}$$

with

$$\mathbf{R}_{\psi_\mathrm{L}} = \begin{bmatrix} \cos\psi_\mathrm{L} & -\sin\psi_\mathrm{L} & 0 \\ \sin\psi_\mathrm{L} & \cos\psi_\mathrm{L} & 0 \\ 0 & 0 & 1 \end{bmatrix}.$$

As the x_h-y_h plane is parallel to the x_n-y_n plane, the angular velocity $\boldsymbol{\omega}_\mathrm{h}$ of the leader's heading coordinate system relative to the NED coordinate system can be represented as $(0, 0, \dot{\psi}_\mathrm{L})$ in the two coordinate systems. This facilitates the estimation of angular velocity $\boldsymbol{\omega}_\mathrm{h}$ from the heading angle measurement ψ_L.

III. Problem Formulation and Solution Scheme

Formation flight can be realized in different ways with different dynamics. For example, it can be realized in a collaboration manner, i.e. the trajectory tracking strategy. The strategy can be illustrated using Fig. 2: Suppose point R be the leader's position reference at a given time t (it is also the reference of the formation team), point D be the follower's desired position at the same moment. Considering the station-keeping constraint, we can then determine the desired position D of the follower via the position reference R of the leader. In other words, both of them are prescribed by (cooperative) path planning. In the ideal case, the team flies in a station-keeping formation configuration. The follower's response is, however, determined only by the reference inputs of the leader, but not affected by the leader's response. As a result, the leader cannot maneuver arbitrarily to keep the formation unchanged.

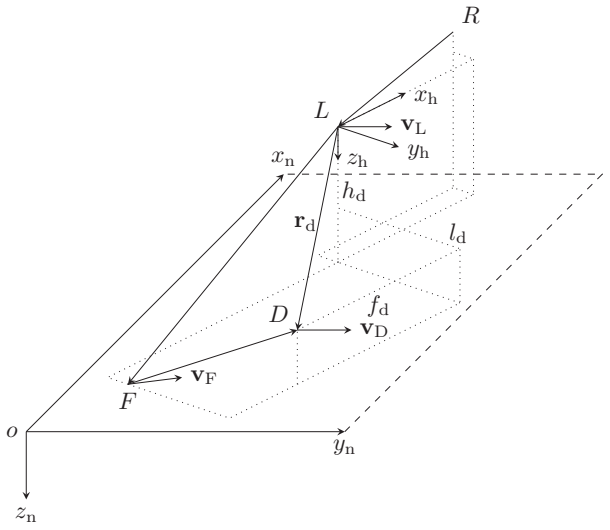

Fig. 2. Three-dimensional formation geometry

Formation flight can also be realized in a cooperation manner. In our work, the leader-follower station-keeping strategy is adopted in both leader mode and front mode. Note that the two modes have no difference in this paper as only two aircraft are utilized in the formation. The strategy can be illustrated in Fig. 2: Let point L be the leader's position response at the given time t, point F be the follower's actual position at the same moment. From the aspect of formation-shape keeping, it is obvious to have the actual separation $\overrightarrow{LF}$ between the leader and the follower coincide with the desired separation $\overrightarrow{LD}$ as close as possible, i.e. the separation error $\overrightarrow{FD} = 0$ at any time regardless of the position difference between R and D. On the other hand, from the aspect of team path tracking, the leader is to track its reference to achieve $\overrightarrow{RL} = 0$ at any time. Formation flight is achieved when both the tracking conditions are met. Therefore, by considering some practical aspects such as wind disturbance, we need two robust and perfect tracking solutions to every aircraft in the formation flight.

In 2000, *Chen et al.* has proposed a solution to this robust tracking problem — the RPT control approach [20]. It utilizes the derivative information $\dot{r}$, $\ddot{r}$, ... of the reference signal r to construct the control inputs so that the controller has the ability to track a given reference signal with arbitrarily fast settling time in the face of external disturbances and initial conditions. For example, Fig. 3 shows an RPT control law (in the dashed box) to the controlled object characterized by double integrators. If we derive the close-loop transfer function from the reference $\mathbf{p}_\mathrm{r}$ to the response $\mathbf{p}$, $\mathbf{p} = \mathbf{p}_\mathrm{r}$ is obtained. In fact, these are the kinematic model of aircraft described in the NED coordinate system and the corresponding control law applied to the outer loop of our unmanned helicopters. Interested readers can refer to [21] for the detailed design process of the tracking control for a single UAV based on the RPT control approach.

For the ease of reference, we depict the two-loop control scheme of our unmanned helicopters in Fig. 4. The inner loop control is mainly to stabilize the attitude of the aircraft and attenuate the wind disturbance, which is designed with H_∞ control technique. The outer loop control focuses on driving the aircraft to track the given path, which is designed with the RPT control technique mentioned above. Besides the usual position reference $\mathbf{p}_\mathrm{r}$, the corresponding velocity $\mathbf{v}_\mathrm{r}$ as well as the acceleration $\mathbf{a}_\mathrm{r}$ information are used as inputs.

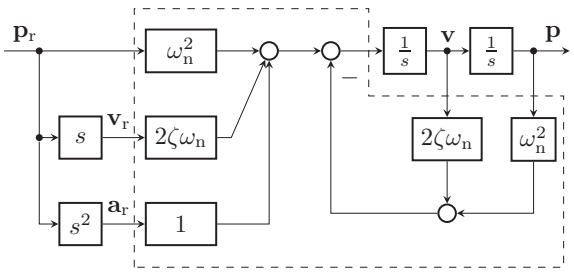

Fig. 3. The robust and perfect tracking control for the outer loop

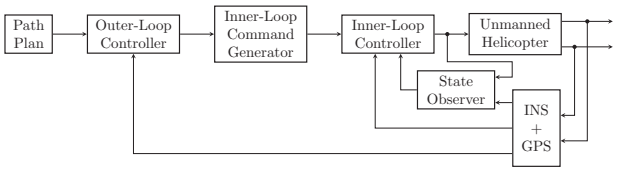

Fig. 4. A two-loop control scheme for a single UAV

IV. Formation Command Generation

Our objective is to minimize the formation error by the reaction of the follower. Thus, the desired inputs of the follower should be derived from the actual state of the leader considering the station-keeping constraint.

A. 3D Formation Dynamics

From a geometric viewpoint (see also Fig. 2), we know

$$\overrightarrow{OD} = \overrightarrow{OL} + \overrightarrow{LD} \tag{2}$$

denoted with vector form

$$\mathbf{p}_\mathrm{D} = \mathbf{p}_\mathrm{L} + \mathbf{r}_\mathrm{d}, \tag{3}$$

where $\mathbf{p}_\mathrm{D}$ and $\mathbf{p}_\mathrm{L}$ are the follower's desired position and the leader's actual position, respectively, and $\mathbf{r}_\mathrm{d}$ is the desired relative separation between the leader and the follower. The above vector equation can be described in the fixed-NED coordinate system as follows

$$\begin{pmatrix} x_\mathrm{D} \\ y_\mathrm{D} \\ z_\mathrm{D} \end{pmatrix} = \begin{pmatrix} x_\mathrm{L} \\ y_\mathrm{L} \\ z_\mathrm{L} \end{pmatrix} + \begin{bmatrix} \cos\psi_\mathrm{L} & -\sin\psi_\mathrm{L} & 0 \\ \sin\psi_\mathrm{L} & \cos\psi_\mathrm{L} & 0 \\ 0 & 0 & 1 \end{bmatrix} \begin{pmatrix} f_\mathrm{d} \\ l_\mathrm{d} \\ h_\mathrm{d} \end{pmatrix}, \tag{4}$$

where the matrix is the rotation transform $\mathbf{R}_{\psi_\mathrm{L}}$, ψ_L is the heading response of the leader, and $(f_\mathrm{d}, l_\mathrm{d}, h_\mathrm{d})$ is the description of $\mathbf{r}_\mathrm{d}$ in the leader's heading coordinate system, i.e. the formation configuration of the follower with respect to the leader. Notice that we study the case with the configuration of $(f_\mathrm{d}, l_\mathrm{d}, h_\mathrm{d})$ fixed in the leader's heading coordinate system.

To fully utilize the RPT control, we need to know the desired translational kinematics of the follower, i.e. the corresponding velocity and acceleration information besides the desired position. With reference to the kinematics of moving reference frames, we differentiate (3) once with respect to time, the desired velocity of the follower is obtained as

$$\begin{aligned} \mathbf{v}_\mathrm{D} &= \dot{\mathbf{p}}_{\mathrm{D}/\mathrm{n}} = \dot{\mathbf{p}}_{\mathrm{L}/\mathrm{n}} + \dot{\mathbf{r}}_{\mathrm{d}/\mathrm{n}} \\ &= \mathbf{v}_\mathrm{L} + \dot{\mathbf{r}}_{\mathrm{d}/\mathrm{h}} + \boldsymbol{\omega}_\mathrm{h} \times \mathbf{r}_\mathrm{d} = \mathbf{v}_\mathrm{L} + \boldsymbol{\omega}_\mathrm{h} \times \mathbf{r}_\mathrm{d}, \end{aligned} \tag{5}$$

where the subscript '$_\mathrm{/n}$' denotes that the differentiation is conducted in the NED coordinate system, the subscript '$_\mathrm{/h}$' denotes that the differentiation is conducted in the leader's heading coordinate system. Thus, $\mathbf{v}_\mathrm{D}$ and $\mathbf{v}_\mathrm{L}$ are the desired velocity of the follower and the actual velocity of the leader, respectively, observed in the NED coordinate system. We should notice $\dot{\mathbf{r}}_{\mathrm{d}/\mathrm{h}} = 0$ since the desired separation $\mathbf{r}_\mathrm{d}$ is unchanged in both magnitude and direction with respect to the leader's heading coordinate system in the station-keeping formation. $\boldsymbol{\omega}_\mathrm{h} = (0, 0, \dot{\psi}_\mathrm{L})$ is the angular velocity of the leader's heading coordinate system with respect to the NED

coordinate system and the term of cross product is induced by their relative rotation. Decomposing the above equation on the NED axes, we have

$$\begin{pmatrix} v_{\mathrm{Dx}} \\ v_{\mathrm{Dy}} \\ v_{\mathrm{Dz}} \end{pmatrix} = \begin{pmatrix} v_{\mathrm{Lx}} \\ v_{\mathrm{Ly}} \\ v_{\mathrm{Lz}} \end{pmatrix} + \mathbf{R}_{\psi_{\mathrm{L}}} \begin{pmatrix} -\dot{\psi}_{\mathrm{L}} l_{\mathrm{d}} \\ \dot{\psi}_{\mathrm{L}} f_{\mathrm{d}} \\ 0 \end{pmatrix}, \tag{6}$$

where $(v_{\mathrm{Dx}}, v_{\mathrm{Dy}}, v_{\mathrm{Dz}})$ and $(v_{\mathrm{Lx}}, v_{\mathrm{Ly}}, v_{\mathrm{Lz}})$ are the descriptions of the follower's desired velocity $\mathbf{v}_{\mathrm{D}}$ and the leader's actual velocity $\mathbf{v}_{\mathrm{L}}$, respectively, in the NED coordinate system. The latter can be measured directly by a GPS/INS (Global Positioning System/Inertia Navigation System) combined navigation system installed on the leader, where the changing rate $\dot{\psi}_{\mathrm{L}}$ of the leader's heading angle can be determined by the body-axis angular rates and Euler angles of the leader according to the Euler kinematic equation,

$$\dot{\psi}_{\mathrm{L}} = q_{\mathrm{L}} \sin\phi_{\mathrm{L}} \sec\theta_{\mathrm{L}} + r_{\mathrm{L}} \cos\phi_{\mathrm{L}} \sec\theta_{\mathrm{L}}. \tag{7}$$

All signals on the right hand side can be measured by an inertia measurement unit (IMU). Notice that we have avoided the singularity at $\theta_{\mathrm{L}} = \pm 90^\circ$ as the UAVs do not fly at this extreme condition in our implementation. Similar to the derivation of the desired velocity, differentiating (5), the desired acceleration of the follower can be obtained,

$$\begin{aligned} \mathbf{a}_{\mathrm{D}} &= \dot{\mathbf{v}}_{\mathrm{D/n}} = \dot{\mathbf{v}}_{\mathrm{L/n}} + \dot{\boldsymbol{\omega}}_{\mathrm{h/n}} \times \mathbf{r}_{\mathrm{d}} + \boldsymbol{\omega}_{\mathrm{h}} \times \dot{\mathbf{r}}_{\mathrm{d/n}} \\ &= \mathbf{a}_{\mathrm{L}} + \boldsymbol{\alpha}_{\mathrm{h}} \times \mathbf{r}_{\mathrm{d}} + \boldsymbol{\omega}_{\mathrm{h}} \times (\dot{\mathbf{r}}_{\mathrm{d/h}} + \boldsymbol{\omega}_{\mathrm{h}} \times \mathbf{r}_{\mathrm{d}}) \\ &= \mathbf{a}_{\mathrm{L}} + \boldsymbol{\alpha}_{\mathrm{h}} \times \mathbf{r}_{\mathrm{d}} + \boldsymbol{\omega}_{\mathrm{h}} \times (\boldsymbol{\omega}_{\mathrm{h}} \times \mathbf{r}_{\mathrm{d}}), \end{aligned} \tag{8}$$

where $\mathbf{a}_{\mathrm{D}}$ and $\mathbf{a}_{\mathrm{L}}$ are the desired acceleration of the follower and the actual acceleration of the leader, respectively, observed in the NED coordinate system. $\boldsymbol{\alpha}_{\mathrm{h}} = (0, 0, \ddot{\psi}_{\mathrm{L}})$ is the angular acceleration of the leader's heading coordinate system with respect to the NED coordinate system. Decomposing the above equation on the NED axes, we have

$$\begin{pmatrix} a_{\mathrm{Dx}} \\ a_{\mathrm{Dy}} \\ a_{\mathrm{Dz}} \end{pmatrix} = \begin{pmatrix} a_{\mathrm{Lx}} \\ a_{\mathrm{Ly}} \\ a_{\mathrm{Lz}} \end{pmatrix} + \mathbf{R}_{\psi_{\mathrm{L}}} \left[\begin{pmatrix} -\ddot{\psi}_{\mathrm{L}} l_{\mathrm{d}} \\ \ddot{\psi}_{\mathrm{L}} f_{\mathrm{d}} \\ 0 \end{pmatrix} - \begin{pmatrix} \dot{\psi}_{\mathrm{L}}^2 f_{\mathrm{d}} \\ \dot{\psi}_{\mathrm{L}}^2 l_{\mathrm{d}} \\ 0 \end{pmatrix} \right], \tag{9}$$

where $\ddot{\psi}_{\mathrm{L}}$ is the angular acceleration of the leader's heading angle. It can be obtained by differentiating (7),

$$\begin{aligned} \ddot{\psi}_{\mathrm{L}} &= \dot{q}_{\mathrm{L}} \sin\phi_{\mathrm{L}} \sec\theta_{\mathrm{L}} + q_{\mathrm{L}} \dot{\phi}_{\mathrm{L}} \cos\phi_{\mathrm{L}} \sec\theta_{\mathrm{L}} \\ &\quad + q_{\mathrm{L}} \dot{\theta}_{\mathrm{L}} \sin\phi_{\mathrm{L}} \frac{\sin\theta_{\mathrm{L}}}{\cos^2\theta_{\mathrm{L}}} + \dot{r}_{\mathrm{L}} \frac{\cos\phi_{\mathrm{L}}}{\cos\theta_{\mathrm{L}}} \\ &\quad - r_{\mathrm{L}} \dot{\phi}_{\mathrm{L}} \frac{\sin\phi_{\mathrm{L}}}{\cos\theta_{\mathrm{L}}} + r_{\mathrm{L}} \dot{\theta}_{\mathrm{L}} \cos\phi_{\mathrm{L}} \frac{\sin\theta_{\mathrm{L}}}{\cos^2\theta_{\mathrm{L}}}. \end{aligned} \tag{10}$$

Notice that $\dot{q}_{\mathrm{L}}$ and $\dot{r}_{\mathrm{L}}$ are not measurable and cannot be derived easily from other measurements. Practically, numerical differentiation is very sensitive to noise. A simple way to avoid differentiation is to omit the term $\boldsymbol{\alpha}_{\mathrm{h}} \times \mathbf{r}_{\mathrm{d}}$ in the acceleration equation (8) as the angular acceleration is zero or very close to zero in non-aggressive flight. Also, we can omit the two terms related to $\dot{q}_{\mathrm{L}}$ and $\dot{r}_{\mathrm{L}}$ in (10). For the latter case, we again utilize the Euler kinematic equations,

$$\dot{\phi}_{\mathrm{L}} = p_{\mathrm{L}} + q_{\mathrm{L}} \sin\phi_{\mathrm{L}} \tan\theta_{\mathrm{L}} + r_{\mathrm{L}} \cos\phi_{\mathrm{L}} \tan\theta_{\mathrm{L}} \tag{11}$$

$$\dot{\theta}_{\mathrm{L}} = q_{\mathrm{L}} \cos\phi_{\mathrm{L}} - r_{\mathrm{L}} \sin\phi_{\mathrm{L}}, \tag{12}$$

where all the signals on the right hand side of the equations can be measured by an IMU. The problem left now is that all the measurements of angular rates (p, q, r) and accelerations are very noisy in practice. In the next subsection, we will design a Kalman filter to estimate the signals $\mathbf{a}_{\mathrm{D}}$, $\dot{\psi}_{\mathrm{L}}$ and $\ddot{\psi}_{\mathrm{L}}$ instead of using the three Euler kinematic equations.

Lastly, the heading direction of the follower should follow the leader's heading during the formation flight. Since heading angle can be set arbitrarily for helicopters, we let

$$\psi_{\mathrm{D}} = \psi_{\mathrm{R}}, \tag{13}$$

i.e. let the desired heading of the follower be the desired heading of the leader.

B. Estimation of Leader Information

To derive the desired position $\mathbf{p}_{\mathrm{D}}$, velocity $\mathbf{v}_{\mathrm{D}}$, and acceleration $\mathbf{a}_{\mathrm{D}}$ of the follower, we need know the leader's actual heading ψ_{L} and its derivatives $\dot{\psi}_{\mathrm{L}}$, $\ddot{\psi}_{\mathrm{L}}$. As mentioned above, it can also be estimated by a Kalman filter. The process can be modeled as (for notation simplicity, the subscript $_{\mathrm{L}}$ has been omitted)

$$\begin{aligned} \dot{\mathbf{x}} &= \begin{pmatrix} \dot{\psi} \\ \ddot{\psi} \\ \psi^{(3)} \end{pmatrix} = \begin{bmatrix} 0 & 1 & 0 \\ 0 & 0 & 1 \\ 0 & 0 & 0 \end{bmatrix} \begin{pmatrix} \psi \\ \dot{\psi} \\ \ddot{\psi} \end{pmatrix} + \begin{pmatrix} w_1 \\ w_2 \\ w_3 \end{pmatrix} \\ &= \mathbf{A}\mathbf{x} + \mathbf{w}, \end{aligned} \tag{14}$$

where $\mathbf{w}$ is the white process noise with normal probability distribution $p(\mathbf{w}) \sim N(0, \mathbf{Q})$ and we assume

$$\mathbf{Q} = \begin{bmatrix} \sigma_1^2 & 0 & 0 \\ 0 & \sigma_2^2 & 0 \\ 0 & 0 & \sigma_3^2 \end{bmatrix}. \tag{15}$$

Here, ψ is the only measurable output, and thus the measurement model is

$$z = [1 \quad 0 \quad 0]\mathbf{x} + v = \mathbf{H}\mathbf{x} + v, \tag{16}$$

where v is the white measurement noise with normal probability distribution $p(v) \sim N(0, \sigma_\psi)$ and it is independent of $\mathbf{w}$. To apply this estimator in the onboard digital system, its discrete-time state transition matrix is derived as

$$\mathbf{F} = \mathrm{e}^{\mathbf{A}t}\big|_{t=\tau} = \begin{bmatrix} 1 & \tau & \frac{1}{2}\tau^2 \\ 0 & 1 & \tau \\ 0 & 0 & 1 \end{bmatrix}, \tag{17}$$

and the discrete-time process noise covariance matrix as

$$\begin{aligned} \mathbf{Q}_{\mathrm{d}} &= \int_0^\tau \mathrm{e}^{\mathbf{A}t} \mathbf{Q} \mathrm{e}^{\mathbf{A}^{\mathrm{T}}t} \mathrm{d}t \\ &= \begin{bmatrix} \sigma_1^2\tau + \frac{\sigma_2^2}{3}\tau^3 + \frac{\sigma_3^2}{20}\tau^5 & \frac{\sigma_2^2}{2}\tau^2 + \frac{\sigma_3^2}{8}\tau^4 & \frac{\sigma_3^2}{6}\tau^3 \\ \frac{\sigma_2^2}{2}\tau^2 + \frac{\sigma_3^2}{8}\tau^4 & \sigma_2^2\tau + \frac{\sigma_3^2}{3}\tau^3 & \frac{\sigma_3^2}{2}\tau^2 \\ \frac{\sigma_3^2}{6}\tau^3 & \frac{\sigma_3^2}{2}\tau^2 & \sigma_3^2\tau \end{bmatrix}, \end{aligned} \tag{18}$$

where τ is the sampling interval of the digital system. Therefore, the following discrete-time Kalman filter is obtained:

- Time update equations (predictor):

$$\hat{\mathbf{x}}_k^- = \mathbf{F}\hat{\mathbf{x}}_{k-1} \tag{19}$$

$$\mathbf{P}_k^- = \mathbf{F}\mathbf{P}_{k-1}\mathbf{F}^{\mathrm{T}} + \mathbf{Q}_{\mathrm{d}} \tag{20}$$

- Measurement update equations (corrector):

$$\mathbf{K}_k = \mathbf{P}_k^- \mathbf{H}^{\mathrm{T}} (\mathbf{H}\mathbf{P}_k^- \mathbf{H}^{\mathrm{T}} + R)^{-1} \quad (21)$$

$$\hat{\mathbf{x}}_k = \hat{\mathbf{x}}_k^- + \mathbf{K}_k (z_k - \mathbf{H}\hat{\mathbf{x}}_k^-) \quad (22)$$

$$\mathbf{P}_k = (\mathbf{I} - \mathbf{K}_k \mathbf{H}) \mathbf{P}_k^-. \quad (23)$$

In implementation, due to the various noise, the linear acceleration $\mathbf{a}_{\mathrm{L}}$ measurement of the leader cannot be used directly, but to be estimated with another Kalman filter. The process and measurement models are

$$\dot{\mathbf{x}} = \begin{pmatrix} \dot{p} \\ \dot{v} \\ \dot{a} \end{pmatrix} = \begin{bmatrix} 0 & 1 & 0 \\ 0 & 0 & 1 \\ 0 & 0 & 0 \end{bmatrix} \begin{pmatrix} p \\ v \\ a \end{pmatrix} + \begin{pmatrix} w_1 \\ w_2 \\ w_3 \end{pmatrix} = \mathbf{A}\mathbf{x} + \mathbf{w} \quad (24)$$

and

$$\mathbf{z} = \begin{pmatrix} p \\ v \end{pmatrix} = \begin{bmatrix} 1 & 0 & 0 \\ 0 & 1 & 0 \end{bmatrix} \begin{pmatrix} p \\ v \\ a \end{pmatrix} + \begin{pmatrix} v_1 \\ v_2 \end{pmatrix} = \mathbf{H}\mathbf{x} + \mathbf{v}, \quad (25)$$

where (p, v, a) is the set of position, velocity, and acceleration along a same NED axis (subscripts are omitted for simplicity). As the measurement noise is vector-valued, its covariance matrix is assumed as

$$\mathbf{R} = \begin{bmatrix} \sigma_{\mathrm{p}}^2 & 0 \\ 0 & \sigma_{\mathrm{v}}^2 \end{bmatrix}. \quad (26)$$

All other formulations are implemented similar to the previous filter.

Finally, combining the equations in this section and the measurements of the leader's states, the desired inputs $(\mathbf{p}_{\mathrm{D}}, \mathbf{v}_{\mathrm{D}}, \mathbf{a}_{\mathrm{D}})$ to the follower are generated based on the leader's actual response to the team reference. These inputs together with ψ_{D} are then fed to the follower. The follower's RPT-based tracking controller will drive it to cooperate with the leader to achieve the station-keeping formation flight (See also Fig. 5).

V. Flight Experiments and System Validation

To validate the applicability of the proposed solution scheme in practice, a variety of formation flight experiments have been conducted using two unmanned helicopters, HeLion and SheLion developed in NUS (see Fig. 1). In this section, two flight test results will be presented. Interested readers can refer to our website for more flight results. Due to the larger random walk of altitude measurement from GPS, the two vehicles are arranged to fly in different heights to ensure the safety of the flight tests.

Fig. 6 shows an intuitive 3D view of an autonomous formation flight scenario. The inner trajectory in red is the response of the leader to its reference path, while the outer trajectory in blue is the response of the follower with reference to its desired path, which was determined according to the former. The flight path consists of two parts: two laps of raceway followed by four cycles of hovering turn. Throughout the flight test, the follower is to stay on the left of the leader with a 10 meters distance. The detail breakdown of the flight mission is shown below:

1) Begin with the raceway flight. The leader starts from the midpoint of the left line segment on the inner track while the follower starts from the midpoint of the left straight line segment on the outer track, both at 2m/s speed along the tracks in clockwise direction;
2) During the semicircle turning of the raceway, the leader keeps a tangential speed of 2m/s on the circular track of 10m radius. The follower accelerates automatically up to 4m/s tangential speed to keep up with the leader while flying in a 20m radius circular track;
3) Back to the line segment of the raceway, the follower has to decelerate automatically back to 2m/s speed, to be the same as the leader;
4) Upon the end of two laps of raceway flight, the vehicles hover for a few seconds;
5) The leader performs a hovering right turn maneuver for four cycles, i.e. spinning around its body-carried z_{n}-axis at about 18°/s. The follower reacts by flying along a circle of 10m radius around the leader at about 6m/s tangential speed to keep itself on the left of the leader;
6) The mission is accomplished after the leader has made four cycles of hovering turn.

Notice that the helicopter with one main rotor cannot do a hovering turn at a fixed point without any movement. In theory, it has to fly in a very small circle as the one on the inner track in Fig. 6. Observing Fig. 6, it is also found that the flight trajectories in different laps do not overlap perfectly. It happens mainly because of the random walk of the GPS signals and the external disturbances such as wind gust. The

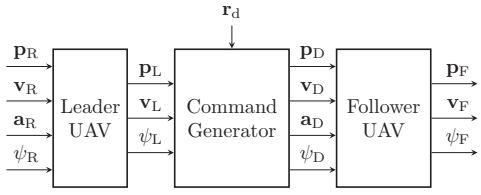

Fig. 5. The RPT-based control scheme of formation flight

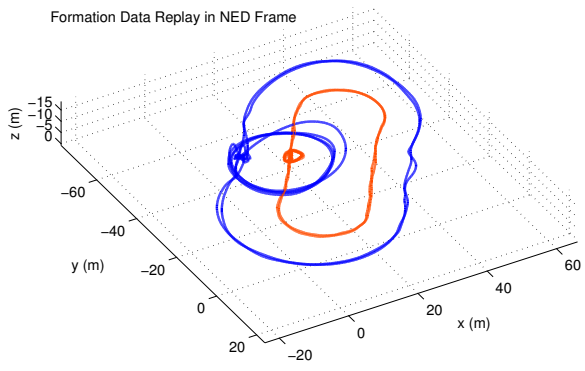

Fig. 6. Three-dimensional view of autonomous formation flight

path tracking errors are, however, negligible as observed from Fig. 7(a) and Fig. 8(a) which are the time histories of the flight trajectories of the leader and the follower, respectively. The references and the responses in these graphs overlap very well, show a good tracking performance. In these results, the RPT control law performs the tracking task nearly without time lag (observing the position responses at the peak times), which is consistent with the theory. In theory, the RPT control technique introduces the dynamics of reference inputs to compensate the trajectory-loop dynamics, which is the main reason that the RPT control approach is utilized in this project.

Fig. 7(b) – 7(d) and Fig. 8(b) – 8(d) are the velocity, attitude, angular rate responses of the leader and the follower, respectively, during the formation flight. Combining them, it is easy to identify the different phases of the flight process. It can be observed easily that the angular rate measurements are very noisy, and hence explained the needs of using the Kalman filters. Fig. 9 depicts the follower's tracking errors in detail, which shows that the position error is mostly in the region of ± 3m (same as the circular error probability radius of the GPS used). The peak at the initial moment is induced by the initial condition of the follower for the formation flight. Another peak between 200s and 250s corresponds to the first cycle of the hovering turn maneuver, in which the follower transits to the hovering turn from a hovering condition. In the steady state, the tracking error decreases to normal level. The last peak at the end of the time history is caused by the sudden stop at the end of hovering turn. In brief, the figures give a very promising performance.

Fig. 10 shows a 3D trajectory of the formation flight scenario in which the unmanned follower tracks the manned leader in forming the letters 'NUS'. The red curve is the

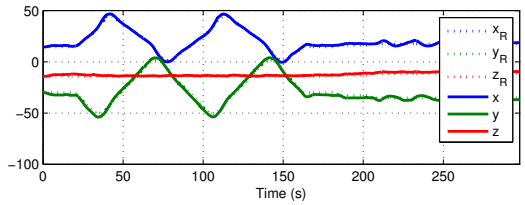

(a) NED-axis position

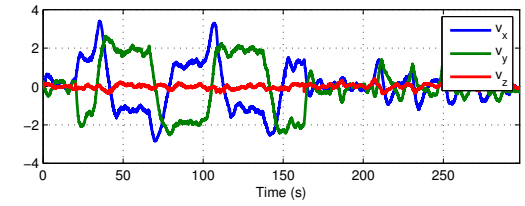

(b) NED-axis velocity

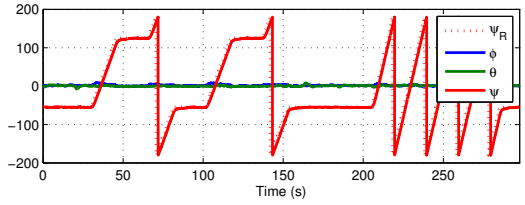

(c) Attitude

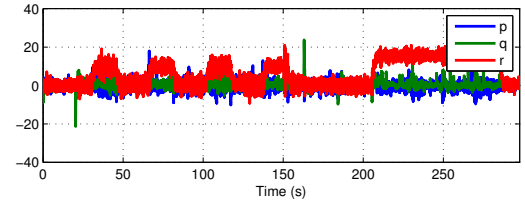

(d) Body-axis angular rate

Fig. 7. Leader's test results of formation flight

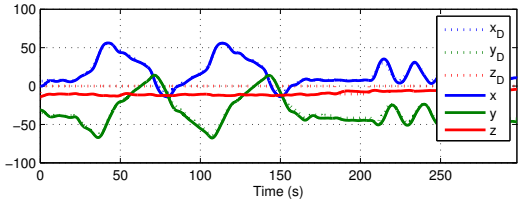

(a) NED-axis position

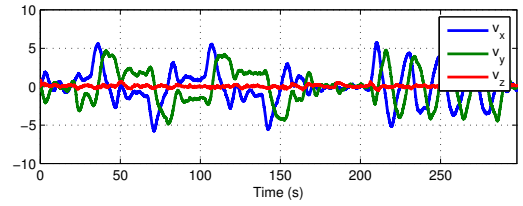

(b) NED-axis velocity

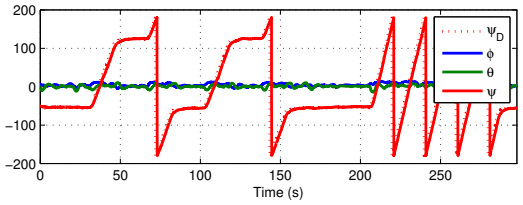

(c) Attitude

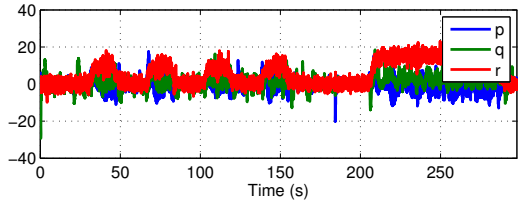

(d) Body-axis angular rate

Fig. 8. Follower's test results of formation flight

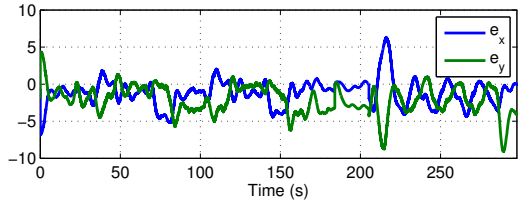

Fig. 9. Formation tracking error of the follower

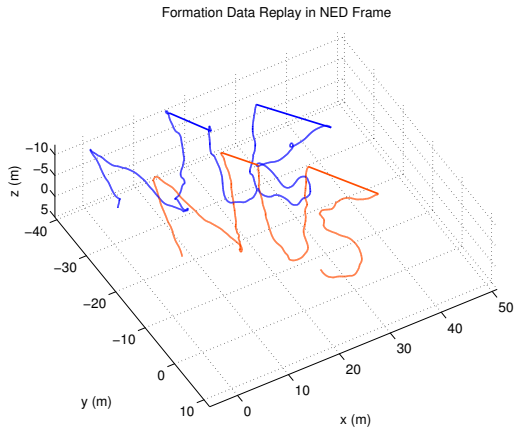

Fig. 10. Three-dimensional view of manned formation flight

trajectory of the leader under manual remote pilot, whereas the blue trajectory is the response of the follower in order for station-keeping. To alleviate the human pilot during the operation, the heading of the aircraft is kept unchanged. With this designed path, forward/backward flight, lateral flight, and slalom flight formations are all tested in a single experiment. The leader helicopter needs an intensive control from the remote pilot to keep balance while tracking the designed path. Notice that in the manual control movement, the acceleration of the vehicle changes more frequently. It increases the effort of the follower to keep the formation configuration different from the previous experiment. Especially on the 'S' path, the leader vehicle keeps changing its acceleration to form the path shape. In other words, flying on this path is far from near trimming flight conditions. Our helicopter is, however, too heavy to perform an aggressive flight due to the bulky avionic system for autonomous flight. It results in the follower did not track the 'S' path perfectly. To save space, the time histories of the position, velocity, attitude and angular rate responses are not given.

On a side note, the communication rate is 10Hz realized by an air-to-air WiFi between the leader and the follower in all the flight experiments.

VI. Concluding Remarks

In this paper, the station-keeping formation flight of two unmanned helicopters is presented. It is cast as two tracking control problems and is solved based on the robust and perfect tracking approach. With this method, no specific formation control loop has been formed, thus the aircraft are versatile and are able to join up or dismiss from a formation configuration easily. The RPT control approach is shown to be an appropriate solution to our formation problem as the overall formation performance is dominated heavily by the tracking loop of the followers. Meanwhile, a Kalman filter-based formation command generator is utilized to provide a better measurement from the leader. Flight test results demonstrate that a promising formation performance can be achieved.

References

[1] Y. Zou, "Distributed control of multiple vehicle systems using constraint forces," Ph.D. Dissertation, Oklahoma State University, Oklahoma, USA, 2008.

[2] I. S. Jeon, J. I. Lee, and M. J. Tahk, "Homing guidance law for cooperative attack of multiple missiles," *Journal of Guidance, Control, and Dynamics*, vol. 33, no. 1, pp. 275–280, 2010.

[3] T. Koishi and T. Murakami, "An approach to cooperative control for formation flight of multiple autonomous helicopters," in *Proceedings of the 35th Annual Conference of the IEEE Industrial Electronics Society*, Porto, Portugal, Nov.3-5, 2009, pp. 1456–1461.

[4] C. Richardson and M. Schoultz, "Formation flight system design concept," in *Proceedings of the 10th IEEE/AIAA Conference on Digital Avionics Systems*, Los Angeles, CA, USA,, Oct.14-17, 1991, pp. 18–25.

[5] J. L. Dargan, M. Pachter, and J. J. D'Azzo, "Automatic formation flight control," in *Proceedings of AIAA Guidance, Navigation, and Control Conference and Exhibit*, Hilton Head Island, SC, USA, Aug.10-12, 1992, pp. 838–857.

[6] S. B. McCamish, M. Pachter, and J. J. D'Azzo, "Optimal formatoin flight control," in *Proceedings of AIAA Guidance, Navigation and Control Conference and Exhibit*, San Diego, CA, USA, Jul.29-31, 1996, pp. 1–17.

[7] A. W. Proud, M. Pachter, and J. J. D'Azzo, "Close formation flight control," in *Proceedings of AIAA Guidance, Navigation, and Control Conference and Exhibit*, Portland, OR, USA, Aug.9-11, 1999, pp. 1231–1246.

[8] C. E. Hanson, J. Ryan, M. J. Allen, and S. R. Jacobson, "An overview of flight test results for a formation flight autopilot," in *Proceedings of AIAA Guidance, Navigation, and Control Conference and Exhibit*, Monterey, California, USA, Aug.5-8, 2002, pp. 1–14.

[9] Y. Gu, G. Campa, B. Seanor, S. Gururajan, and M. R. Napolitano, "Autonomous formation flight: Design and experiments," in *Aerial Vehicles*, T. M. Lam, Ed. Croatia: InTech, 2009, pp. 235–258.

[10] A. Pant, P. Seiler, T. J. Koo, and K. Hedrick, "Mesh stability of unmanned aerial vehicle clusters," in *Proceedings of the American Control Conference*, Arlington, VA, USA, Jun.25-27, 2001, pp. 62–68.

[11] U. Pilz, A. P. Popov, and H. Werner, "Robust controller design for formation flight of quad-rotor helicopters," in *Proceedings of Joint 48th IEEE Conference on Decision and Control and 28th Chinese Control Conference*, Shanghai, P. R. China, Dec.16-18, 2009, pp. 8322–8327.

[12] F. Fahimi, "Full formation control for autonomous helicopter groups," *Robotica*, vol. 26, no. 2, pp. 143–156, 2008.

[13] J. A. Guerrero, I. Fantoni, S. Salazar, and R. Lozano, "Flight formation of multiple mini rotorcraft via coordination control," in *Proceedings of IEEE International Conference on Robotics and Automation*, Anchorage, Alaska, USA, May3-8, 2010, pp. 620–625.

[14] M. Saffarain and F. Fahimi, "Control of helicopters' formation using non-iterative nonlinear model predictive approach," in *Proceedings of American Control Conference*, Washington, USA, Jun.11-13, 2008, pp. 3707–3712.

[15] S. N. Singh, R. Zhang, P. Chandler, and S. Banda, "Decentralized adaptive close formation control of uav's," in *Proceedings of the 39th AIAA Aerospace Sciences Meeting and Exhibit*, Reno, NV, USA, Jan.8-11, 2001, pp. 1–11.

[16] F. Giulietti, L. Pollini, and M. Innocenti, "Autonomous formation flight," *IEEE Control Systems Magazine*, vol. 20, no. 6, pp. 34–44, 2000.

[17] ——, "Formation flight control: A behavioral approach," in *Proceedings of AIAA Guidance, Navigation, and Control Conference and Exhibit*, Montreal, Canada, Aug.6-9, 2001, pp. 1–5.

[18] J. M. Fowler and R. D'Andrea, "A formation flight experiment," *IEEE Control Systems Magazine*, vol. 23, no. 5, pp. 35–53, 2003.

[19] L. J. L. Hinchman, "Distributed control: A path riddled with challenges," in *Proceedings of the 1st AIAA Technical Conference and Workshop on Unmanned Aerospace Vehicles*, Portsmouth, Virginia, USA, May20-23, 2002.

[20] B. M. Chen, *Robust and H_∞ Control*, ser. Communications and Control Engineering. London, UK: Springer-Verlag, 2000.

[21] B. Wang, B. M. Chen, and T. H. Lee, "An RPT approach to time-critical path following of an unmanned helicopter," in *Proceedings of the 8th Asian Control Conference*, Kaohsiung, Taiwan, May15-18, 2011, pp. 211–216.